Journal of Controlled Release 293 (2019) 126–134

Contents lists available at ScienceDirect

Journal of Controlled Release

journal homepage: www.elsevier.com/locate/jconrel

In vivo stability of supramolecular host–guest complexes monitored by dual-isotope multiplexing in a pre-targeting model of experimental liver radioembolization

Mick M. Welling[a], Silvia J. Spa[a], Danny M. van Willigen[a], Daphne D.D. Rietbergen[a,b], Meta Roestenberg[c], Tessa Buckle[a], Fijs W.B. van Leeuwen[a,d,*]

[a] *Interventional Molecular Imaging Laboratory, Department of Radiology, Leiden University Medical Center, Leiden, the Netherlands*
[b] *Section Nuclear Medicine, Department of Radiology, Leiden University Medical Center, Leiden, the Netherlands*
[c] *Department of Parasitology and Department of Infectious diseases, Leiden University Medical Center, Leiden, the Netherlands*
[d] *Laboratory of BioNanoTechnology, Department of Agrotechnology and Food Sciences, Wageningen University, Wageningen, the Netherlands*

ARTICLE INFO

Keywords:
Radioembolization
Interventional radiology
Supramolecular chemistry
Dual-labeling
Pre-targeting
Theranostics

ABSTRACT

Introduction: Cyclodextrin (CD)-based supramolecular interactions have been proposed as nanocarriers for drug delivery. We previously explored the use of these supramolecular interactions to perform targeted hepatic radioembolization. In a two-step procedure the appropriate location of the diagnostic pre-targeting vector can first be confirmed, after which the therapeutic vector will be targeted through multivalent host–guest interactions. Such a procedure would prevent therapeutic errors that come from a mismatch between diagnostic and therapeutic procedures. In the current study we explored the use of dual-isotope imaging to assess the *in vivo* stability of the formed complex and individual components.

Methods: Dual-isotope imaging of the host and guest vectors was performed after labeling of the pre-targeted guest vector, being adamantane (Ad) functionalized macro-aggregated albumin (MAA) particles, with technetium-99 m (^{99m}Tc-MAA-Ad). The host vector, $Cy5_{0.5}CD_9PIBMA_{39}$, was labeled with indium-111 (^{111}In-$Cy5_{0.5}CD_9PIBMA_{39}$). The *in situ* stability of both the individual vectors and the resulting [MAA-Ad–^{111}In-$Cy5_{0.5}CD_9PIBMA_{39}$] complexes was studied over 44 h at 37 °C in a serum protein-containing buffer. *In vivo*, the host vector ^{111}In-$Cy5_{0.5}CD_9PIBMA_{39}$ was administered two hours after local deposition of ^{99m}Tc-MAA-Ad in mice. Dual-isotope SPECT imaging and quantitative biodistribution studies were performed between 2 and 44 h post intravenous host vector administration.

Results: The individual vectors portrayed < 5% dissociation of the radioisotope over the course of 20 h. Dissociation of [MAA-Ad–^{111}In-$Cy5_{0.5}CD_9PIBMA_{39}$] complexes remained within a 10–20% range after incubation in serum. *In vivo* dual-isotope SPECT imaging of host–guest interactions revealed co-localization of the tracer components. Quantitative assessment of the biodistribution revealed that the hepatic accumulation of the host vector nearly doubled between 2 h and 44 h post-injection (from 14.9 ± 6.1%ID/g to 26.2 ± 2.1%ID/g).

Conclusions: Assessment of intra-hepatic host–guest complexation was successfully achieved using dual isotope multiplexing, underlining the complex stability that was found *in situ* (up to 44 h in serum). Overall, the results obtained in this study highlight the potential of supramolecular chemistry as a versatile platform that could advance the field of nanomedicine.

1. Introduction

Hepatocellular carcinoma (HCC) and liver metastases of colorectal cancer (mCRC) are the third most common cause of cancer-related deaths worldwide [1,2]. With currently 1.12 million deaths worldwide per year, both the incidence of these cancer types and their impact on health expenditure is increasing. Surgical excision is considered the fist-line therapy but cannot be applied in grade 3–5 staged HCC. The substantial portion of inoperable patients that present metastatic liver tumors are therefore in need of alternative treatment strategies [3–5]. One relatively novel treatment option that has presented potential to effectively manage these hepatic tumors is radio- or chemo-

* Corresponding author.
E-mail address: F.W.B.van_Leeuwen@lumc.nl (F.W.B. van Leeuwen).

https://doi.org/10.1016/j.jconrel.2018.11.020
Received 3 September 2018; Received in revised form 20 November 2018; Accepted 21 November 2018
Available online 25 November 2018
0168-3659/

embolization [6]; of these two radioembolization is the most frequently applied. In HCG patients this embolization strategy has proven to be beneficial to survival in patients with HCG [7].

Radioembolization is performed using a two-step interventional radiological theranostic procedure. In this procedure Single Positron Emission Computed Tomography (SPECT) imaging of macro-aggregated albumin (scout scan delivered by a CT guided catheter; ^{99m}Tc-MAA; d = 10–40 μm) is used to explore the potential of selective internal radiotherapy (*i.e.*, radioembolization). When correct localization of the ^{99m}Tc-MAA is visualized, therapeutic β-emitting microparticles (d = 15–25 μm) [8] containing ^{90}Y (SIR-Spheres®, Sirtex; Therasphere, BTG®) or ^{166}Ho (QuiremSpheres; Quirem Medical) are injected two weeks later *via* the same positioned catheter in the *A. hepatica* [9]. The overlap in size and retention properties between the albumin macro-aggregates and the microparticles has been sufficient for the clinical guidelines to define a ^{99m}Tc-MAA scout scan as a standard requirement to predict accurate delivery of therapeutic microspheres during a second intervention. Despite this inclusion in the guidelines, a mismatch between the scout scan and therapy delivery which can lead to adverse side effects and suboptimal dose delivery [6] is seen in 30% of the cases [10–12]. This indication signifies a need for innovative solutions that help refine the correlation between the two interventions (*i.e.*, the scout scan and therapeutic delivery). Another drawback is the delay (≈ 14 days) between the execution of the scout scan and the therapeutic intervention that mainly occurs as result of the production/delivery time of the β-emitting microspheres [9].

While some groups have proposed to use low-dose application of therapeutic microspheres during scout scans [13], we have previously explored an alternative route based on the use of a pre-targeting strategy. In this latter approach, the agent used to create a diagnostic scout scan provides the target for a secondary agent containing the therapeutic component. As proof of concept we explored cyclodextrin (CD)-based host and adamantane (Ad) guest interactions on a MAA platform [14]. When functionalized with Ad guest-moieties (yielding MAA-Ad; guest vector), the compound used for the diagnostic scout scan, could be used as the target for a secondary CD-containing host vector, which is in this case was a ^{99m}Tc-labeled CD-functionalized Poly (isobutylene-*alt*-maleic-anhydride) polymer (^{99m}Tc-Cy5$_n$CD$_n$PIBMA$_n$"). The encouraging *in vivo* data obtained with this set-up indicated that supramolecular host–guest interactions could provide an alternative procedure for radioembolization [15].

In the work presented here we expand our previous efforts by studying the stability of the host–guest complexes over a period that matches the timespan of the clinical radioembolization procedure. Dual-isotope SPECT imaging (see Scheme 1) was used to individually track both the host (CD-functionalized polymer labeled with Cy5 and ^{111}In ($t_{1/2}$ = 2.9 d, 170 & 240 KeV)) and guest (MAA-Ad radiolabeled with ^{99m}Tc ($t_{1/2}$ = 6 h, 140 KeV)) vector [16]. To evaluate the integrity of the individual compounds and the host–guest complexes formed, *in vitro* and *in vivo* stability studies were related to *in vivo* SPECT imaging and quantitative biodistribution patterns of both components. These longitudinal assessments were then used to determine the chemical refinements that are required to contemplate translation of the technology into the clinic.

2. Materials and methods

General analytical procedures and information on the materials used are provided in the Supporting Information (SI).

3. Synthesis and analysis

Synthesis and characterization of both adamantane-tetrafluorophenol (Ad-TFP) and β-cyclodextrin-poly(isobutylene-*alt*-maleic-anhydride) (Cy5$_{0.5}$CD$_9$PIBMA$_{39}$, ~18.7 kDa, d ≈ 11.7 nm) were carried out as previously described [14,15].

3.1. Radiolabeling of host vector MAA(−ad) with technetium-99 m and stability assay

Labeling of macro-aggregated albumin (MAA) with technetium (^{99m}Tc-MAA) and functionalization with Ad-TFP was carried out as described previously [15]. The stability of the ^{99m}Tc-chelation was determined in fetal calf serum (FCS, Life Technologies Inc. CA) after 2, 4, and 20 h. The release of radioactivity was determined after centrifugation and two subsequent washing steps with PBS (3 min, 1500 × g), as described previously [15].

3.2. Labeling of Cy5$_{0.5}$CD$_9$PIBMA$_{39}$ with indium-111 (^{111}In-Cy5$_{0.5}$CD$_9$PIBMA$_{39}$) and stability assay

The host vector, Cy5$_{0.5}$CD$_9$PIBMA$_{39}$, containing an abundance of freely available carboxylic acid moieties, was radiolabeled with indium-111. To 10 μL of Cy5$_{0.5}$CD$_9$PIBMA$_{39}$ (1 mg/mL PBS) ammonium acetate (0.25 M, pH 5; 40 μL) was added followed by 25–150 μL of an acidic solution of ^{111}InCl$_3$ (370 MBq/mL, Mallinckrodt Medical, Petten, The Netherlands). This mixture was gently shaken in the dark for 1 h at 37 °C. Hereafter, the pH was adjusted to 7.5 in PBS. The radiochemical

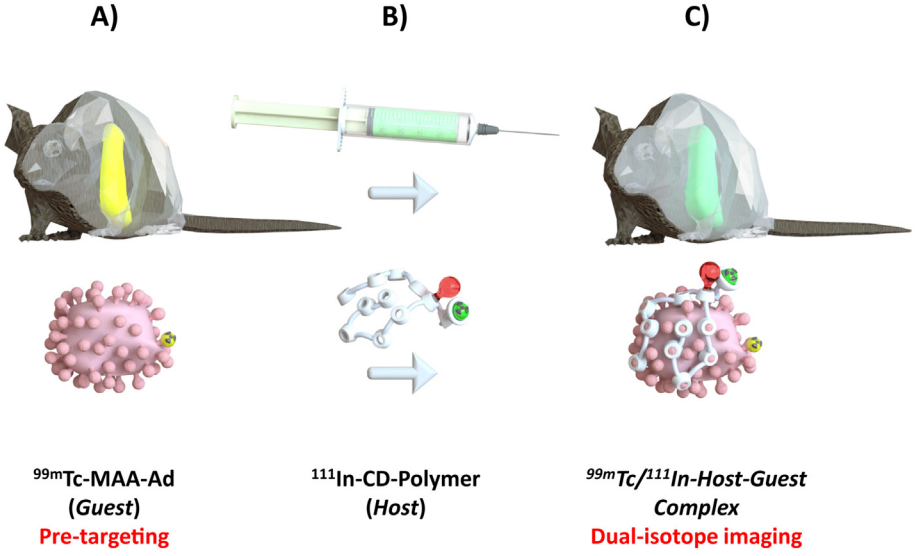

Scheme 1. Representation of the pre-targeting radioembolization concept: A) Firstly, ^{99m}Tc-MAA-Ad was administered into the liver of a mouse. B) After 2 h, an ^{111}In- Cy5$_{0.5}$CD$_9$PIBMA$_{39}$ was intravenously administered. C) Dual-isotope imaging was performed to assess the co-localization of both compounds at various intervals until 44 h p.i. adamantane (Ad; guest), ^{99m}Tc-labeled and Ad-functionalized macro-aggregated albumin (^{99m}Tc-MAA-Ad; guest vector), cyclodextrin (CD), cyclodextrin functionalized poly(isobutylene-*alt*-maleic-anhydride polymer (Cy5$_{0.5}$CD$_9$PIBMA$_{39}$, host vector), ^{111}In- Cy5$_{0.5}$CD$_9$PIBMA$_{39}$ (radiolabeled host vector).

purity of ^{111}In-Cy5$_{0.5}$CD$_9$PIBMA$_{39}$ was determined at 1 and 20 h by instant thin layer chromatography (ITLC) on 1 × 7 cm ITLC-SG paper strips (Agilent Technologies, USA) with ammonium acetate (0.25 M, pH 5) as mobile phase.

The serum stability of the ^{99m}Tc chelation was determined in fetal calf serum (FCS, Life Technologies Inc. CA). After 24 h, the release of radioactivity was determined with centrifugation and washing steps as described above. To determine the stability in FCS, ^{111}In-Cy5$_{0.5}$CD$_9$PIBMA$_{39}$ was diluted in FCS (2.5 μg/mL) and shaken in a water bath at 37 °C for 20 h. After 2, 4, and 20 h, samples of 0.1 mL were taken, and the release of radioactivity was assessed by ITLC. For comparison, a similar assay was performed for ^{111}In-Cy5$_{0.5}$CD$_9$PIBMA$_{39}$ [15].

3.3. In vitro host–guest interactions and complex stability

In line with previous studies [15], *in vitro* evidence for the host–guest complex formation between MAA-Ad and ^{111}In-Cy5$_{0.5}$CD$_9$PIBMA$_{39}$ was provided by comparing the ^{111}In-Cy5$_{0.5}$CD$_9$PIBMA$_{39}$ binding to MAA-Ad and non-functionalized MAA (control). Mixtures of 0.1 mL containing either MAA-Ad or MAA (0.1 mg/mL) with 0.1 mL ^{111}In-Cy5$_{0.5}$CD$_9$PIBMA$_{39}$ (10 μg/mL, 1 MBq) were prepared in 0.8 mL PBS and the solutions were incubated for 1 h in a shaking water bath at 37 °C. After spinning twice and washing with PBS for 5 min at 1500 × g, the decay-corrected radioactivity of the pellet and supernatant was measured in a dose calibrator. Following correction for background activity, the host–guest interaction was expressed as the percentage of the total amount of radioactivity (% binding).

For stability measurements, either 0.1 mL MAA-Ad (0.1 mg/mL) with 0.1 mL ^{111}In-Cy5$_{0.5}$CD$_9$PIBMA$_{39}$ (10 μg/mL, 1 MBq) or 0.1 mL ^{99m}Tc-MAA-Ad (0.1 mg/mL, 1 MBq) with 0.1 mL Cy5$_{0.5}$CD$_9$PIBMA$_{39}$ (10 μg/mL) were prepared as described above and after removal of non-complexed materials the complex was diluted in either 0.8 mL PBS or FCS and incubated for 44 h in a shaking water bath at 37 °C. Following incubation (t = 2, 20, and 44 h), 0.1 mL samples were diluted in 1 mL of PBS and centrifuged for 5 min at 1500 × g. The decay-corrected radioactivity of both the pellet and supernatant was measured in a dose calibrator. Hereby, the radioactivity of the pellet represented association of Cy5$_{0.5}$CD$_9$PIBMA$_{39}$ to MAA-Ad (expressed as % of binding).

4. Imaging experiments

4.1. Animals

In vivo studies were performed using 2–4-month-old Swiss mice (20–35 g, Crl:OF1 strain, Charles River Laboratories, USA). All animal studies were approved by the institutional Animal Ethics Committee (DEC permit 12,160) of the Leiden University Medical Center. Mice were kept under specific pathogen-free conditions in the animal housing facility of the Leiden University Medical Center. Food and water were provided *ad libitum*.

4.2. Animal model and tracer administration

An embolization set-up of the liver was performed according to previously described procedures [15,17]. In brief, ^{99m}Tc-MAA-Ad (0.1 mg/mL, 2–5 MBq, n = 6) was injected into the spleen of the mice (embolization step). Two hours after embolization, a second injection with ^{111}In-Cy5$_{0.5}$CD$_9$PIBMA$_{39}$ (1 μg, 10 MBq) was administered intravenously. Mice were imaged at 2, 12, 20, or 44 h after the second injection using SPECT and fluorescence imaging, where after mice were killed and tissues excised for use in quantitative biodistribution studies (see SPECT and fluorescence imaging protocols and biodistribution studies described below). Non-functionalized ^{99m}Tc-MAA (0.1 mg/mL, 2–5 MBq, n = 6) or merely PBS (n = 3) served as control.

4.3. General SPECT imaging

SPECT imaging was performed as previously described [15] using a three-headed U-SPECT-2 (MILabs, Utrecht, the Netherlands) at various intervals post-injection (p.i.) of the host vector, while being under continuous 1–2% isoflurane anesthesia [18]. Radioactivity counts (range 0–600 keV) from total-body scans were acquired for 30 min. For reconstruction from list mode data, the photo peak energy window was centered at 140 keV (for technetium-99 m) or 240 keV (for indium-111) with a window width of 20%. Longitudinal differences in ^{111}In accumulation in mice were quantified by calculating radioactivity counts in regions of interest (ROI's). For this purpose, on the reconstructed images, using AMIDE's Medical Image Data Examiner (http://amide.sourceforge.net). ROI's were drawn over various tissues (including bone and joints as these were not assessed with routine biodistribution studies) allowing to determine radioactive counts in various tissues over time in a single mouse. ROI's drawn over the jugular veins were taken as a representative for the radioactivity in blood values. After imaging, mice were euthanized and the organs were removed, weighed and the amount of radioactivity present in each organ was quantified to determine the percentage of injected dose per gram tissue (%ID/g). Blood samples obtained prior to sacrifice were counted for radioactivity to determine the clearance from the blood fraction (expressed as the pharmacological half-life $t_{1/2}$) was calculated using GraphPad Prism version 5.01 for Windows (GraphPad Software, San Diego CA, USA).

4.4. Fluorescence imaging protocol

Macroscopic assessment of the fluorescence signal of Cy5$_{0.5}$CD$_9$PIBMA$_{39}$ present in the excised tissues was evaluated using a preclinical IVIS Spectrum imaging system (Caliper Life Science, Hopkinton, MA). Images were acquired following excitation at 640 nm, and light was collected > 680 nm (acquisition time 5 s). Quantitative analysis of the fluorescence present in the tissues (photons/s/cm^2) was performed using the Living Image software from Xenogen v 3.2 (Caliper LS) at equal image adjustment settings.

4.5. Statistical analysis

All data are presented as mean value (± SD) of 3–6 independent measurements. Statistical analysis for differences between groups in the animal studies were performed by with Student's two-tailed independent samples t-test. Significance was assigned for p-values < 0.05. All analyses and calculations were performed using Microsoft® Office Excel 2010 and GraphPad Prism version 5.01 for Windows (GraphPad Software, San Diego, CA, USA).

5. Results

5.1. Radiolabeling, functionalization, and stability of the vectors

Radiolabeling of guest vector with technetium-99 m for 1 h at 37 °C yielded 92.8 ± 3.8% binding of the total added radioactivity. After incubating ^{99m}Tc-MAA in FCS at 37 °C for 20 h the release of radioactivity was shown to be < 5%. Labeling of ^{111}In to Cy5$_{0.5}$CD$_9$PIBMA$_{39}$ for 1 h at 37 °C yielded 95.6 ± 3.6% of binding of the total added radioactivity determined by instant thin layer chromatography (ITLC). To determine the chelation stability, the host vector was incubated in FCS at 37 °C for 20 h. As depicted in Fig. 1A the amount of ^{111}In-activity dissociating from the host after incubating in serum at 37 °C for 20 h was about 5% which indicates that the labeling was robust.

5.2. In vitro host–guest interactions

Host–guest supramolecular interactions *in vitro* increased complexation of the ^{111}In-Cy5$_{0.5}$CD$_{10}$PIBMA$_{39}$ to MAA-Ad by nearly two-

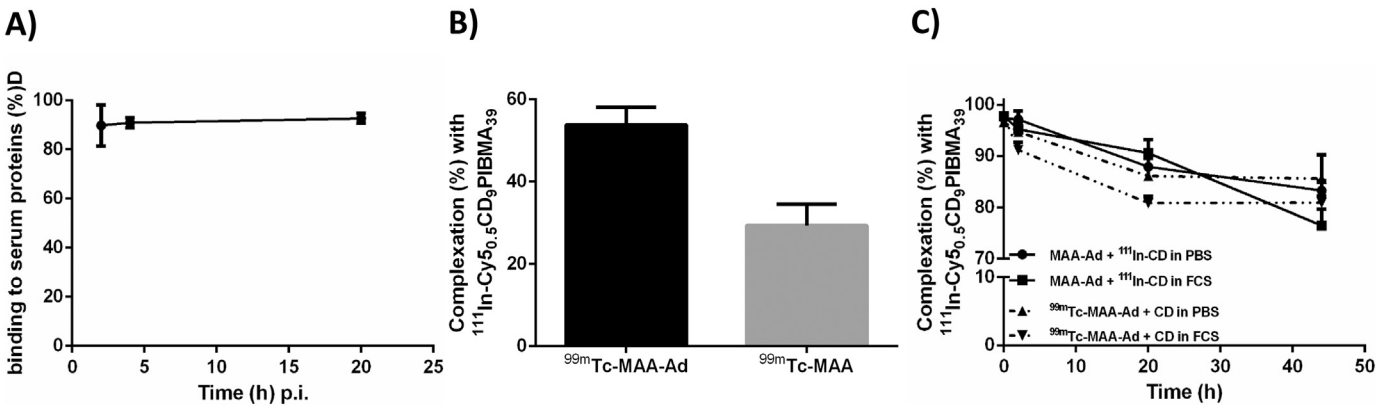

Fig. 1. A) Serum binding of ^{111}In-Cy5$_{0.5}$CD$_9$PIBMA$_{39}$ over 20 h at 37 °C. B) *In vitro* host–guest complexation between guest vectors (MAA-Ad or MAA) and the host vector (^{111}In-Cy5$_{0.5}$CD$_9$PIBMA$_{39}$) after 1 h at 37 °C. Data are expressed as the mean ± SD of the percentage of binding. C) *In vitro* stability determined at 37 °C of the host–guest complexation between guest vector MAA-Ad with host vector ^{111}In-Cy5$_{0.5}$CD$_9$PIBMA$_{39}$ in PBS or FCS (straight lines) and ^{99m}Tc-MAA-Ad with Cy5$_{0.5}$CD$_9$PIBMA$_{39}$ in PBS or FCS (dashed lines). Values are expressed as the % of radioactivity associated with the washed pellet.

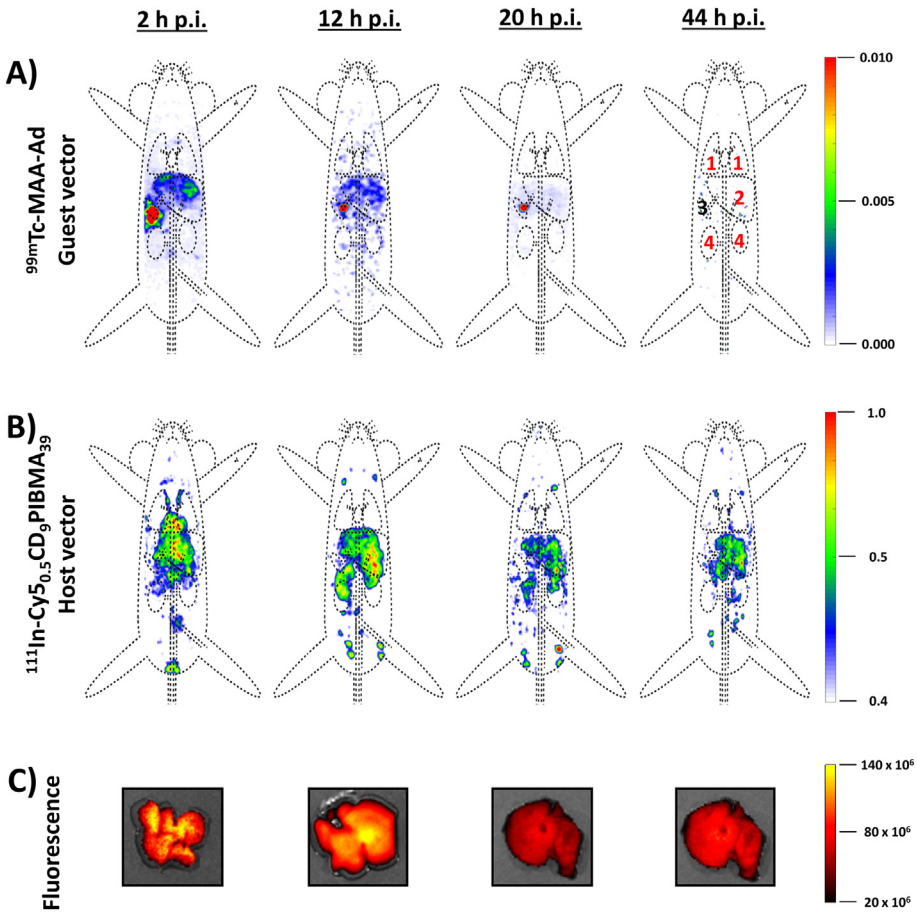

Fig. 2. Time-related (2, 12, 20 and 44 h p.i.) dual-isotope SPECT biodistribution of A) intrasplenic administration of guest vector ^{99m}Tc-MAA-Ad and B) intravenously administered host vector ^{111}In-Cy5$_{0.5}$CD$_9$PIBMA$_{39}$. Organs are marked as (1) lungs, (2) liver, (3) spleen, and (4) kidneys. The scale bars indicate the intensity of radioactivity expressed as arbitrary units. p.i. = post-injection.

fold as compared to what was achieved with non-Ad-functionalized MAA (53.8 ± 4.3% *vs* 29.4 ± 5.1% respectively; $p < 0.001$, $n = 8$; Fig. 1B). This indicates that host–guest interactions influence the complex formation. After 44 h incubation in either PBS or FCS, complex dissociation was found to be in the 10–20% range (see Fig. 1C).

5.3. *In vivo host–guest complex formation*

To further validate the use of a supramolecular pre-targeting concepts during liver radioembolization, a non-tumor bearing animal model was used. The embolization setup in the liver was performed according to previously described procedures [15,17]. The most important reason for choosing this approach is that hepatic catherization in mice is invasive and would have resulted loss of many mice because of heavy bleedings. These bleeding would, in turn, have resulted in radioactive contaminations.

Dual-isotope SPECT imaging facilitated *in vivo* monitoring of host–guest interactions between ^{111}In-Cy5$_{0.5}$CD$_9$PIBMA$_{39}$ and ^{99m}Tc-MAA-Ad. The 6 h half-life of ^{99m}Tc meant its distribution could only be reliably monitored up to 20 h p.i. by means of SPECT imaging (Fig. 2A). Biodistribution studies displayed residual ^{99m}Tc-MAA-Ad activity in the spleen (injection site; amounting to 80.4 ± 23.2%ID/g, 64.2 ± 5.6%

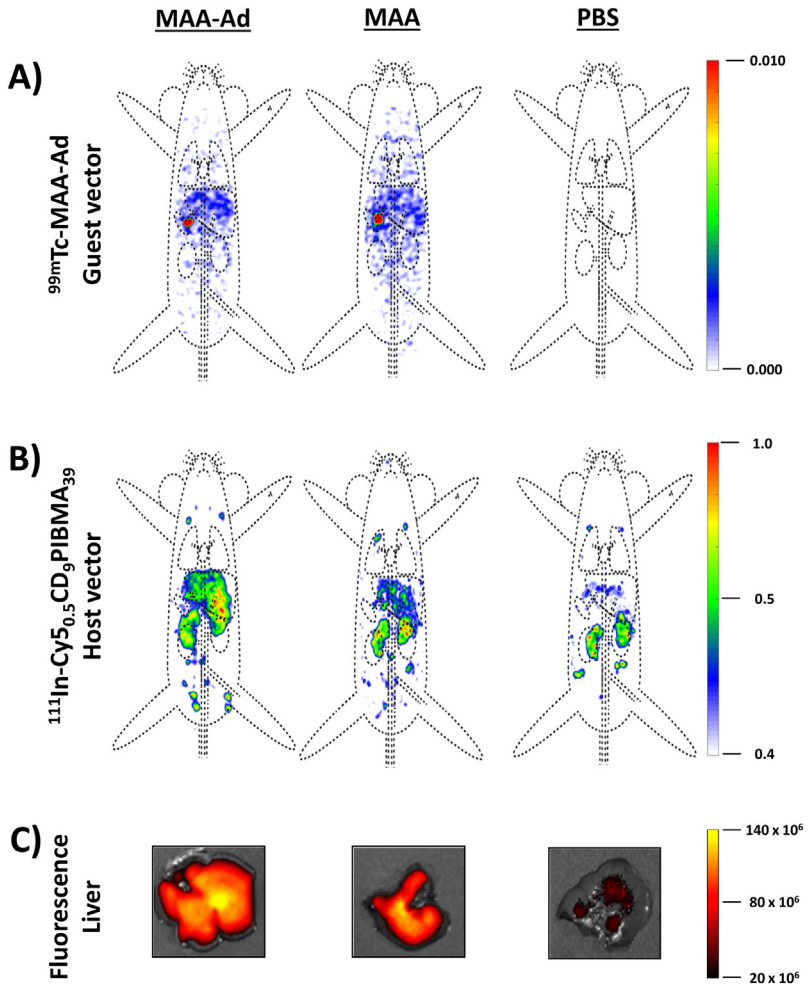

Fig. 3. A) Dual-isotope SPECT biodistribution at 12 h p.i. of the pretargeted guest vector ^{99m}Tc-MAA-Ad. Mice, pretargeted with either non-functionalized ^{99m}Tc-MAA or PBS are used for comparison. Organs are marked as described in Fig. 2. B) Biodistribution of host vector ^{111}In-Cy5$_{0.5}$CD$_9$PIBMA$_{39}$ after intravenous administration. C) Uptake of the host vector ^{111}In-Cy5$_{0.5}$CD$_9$PIBMA$_{39}$ in the liver determined by *ex-vivo* fluorescence imaging at equal settings. The scale bar indicates the intensity of fluorescence expresses as photons/s/cm^2.

ID/g, and 57.9 ± 8.4%ID/g at 2, 12, and 20 h p.i. respectively) and demonstrated prolonged diffusion of the radioactive signal from the spleen to the liver (amounting to 13.2 ± 2.2%ID/g, 36.4 ± 5.3%ID/g, and 43.0 ± 20.2%ID/g at 2, 12, and 20 h p.i., respectively; Fig. S1).

Host–guest complexation between ^{111}In-Cy5$_{0.5}$CD$_9$PIBMA$_{39}$ and ^{99m}Tc-MAA-Ad was monitored *in vivo* by dual-isotope SPECT imaging. Fig. 2B shows the distribution of the host vector in mice pretargeted with guest vector at 2, 12, 20 or 44 h p.i. of the host vector SPECT imaging of ^{111}In displayed the biodistribution of the host vector. As a result of the 2.8 d half-life of ^{111}In, the time-related uptake of the host vector in the liver of mice could be studied up to 44 h p.i. Longitudinal differences in ^{111}In accumulation were quantified either by calculating radioactivity counts in ROI's (Fig. 4A–F) or as quantitative biodistribution studies (see Fig. 5A & Table S1). These analyses revealed that at 20 h p.i. the hepatic uptake of the host vector was at its maximum (approximately 27%ID/g). The observed intestinal uptake of ^{111}In-isotopes (Table S2) is indicative for hepatic uptake followed by intra-intestinal secretion. From 2 h onwards we observed small amounts of ^{111}In accumulation in the shoulder joints, knee joints, pelvis, kidney, and diffuse uptake in bone (Fig. 2B, Fig. 3B, Fig. 4D), but bone uptake remained unchanged over time (Fig. 2A, B, Fig. 4D). Given the concurrence with known reservoirs for free $^{111}In^{3+}$ [19–21], the isotope is most likely dissociated from the carboxylic acid moieties on the polymer backbone. Our results indicate that both methods, either by ROI's or biodistribution assays, provide an accurate representation of the accumulation of the host vector in various tissues in mice. Lung shunting, an essential property to prevent side effects due to off-target delivery [2,11], was not observed at any time point.

Liver uptake was increased by nearly 3-fold in mice treated with the functionalized pre-targeting vector ($p < 0.01$) as compared to the liver uptake of the host vector in control mice injected with ^{99m}Tc-MAA (10.8 ± 4.7%ID) or PBS (8.6 ± 3.1%ID; Fig. 3B & Table S1, Fig. 4B). Despite the presence of ^{99m}Tc-MAA(−Ad) signal in the spleen (see Fig. 3A), accumulation of host vector in this organ was equal to that in PBS controls (Fig. 4B & Table S1). Whether the hepatic uptake of the host vector in the animals that received ^{99m}Tc-MAA depended on non-specific interaction with MAA (as was measured *in vitro*Fig. 1B) or because of the clogging of the microvasculature by MAA particles was undeterminable.

Another interesting observation is the shorter blood half-life ($t_{1/2}$ = 192 min) calculated for the host vector in mice pre-targeted with guest vector ^{99m}Tc-MAA-Ad compared to the half-life of the host vector in mice pretargeted with control guest vector ^{99m}Tc-MAA ($t_{1/2}$ = 306 min) or PBS ($t_{1/2}$ = 318 min) (Table S2). The uptake of ^{111}In activity in other tissues, *e.g.*, blood, heart, lungs, muscle, and brains showed a decrease in uptake of ^{111}In radioactivity over time which was comparable between the two guest vectors or PBS (Table S1), most likely as a result of the clearance of ^{111}In-Cy5$_{0.5}$CD$_9$PIBMA$_{39}$ from these tissues. At all intervals liver-to-blood ratios for mice pre-targeted with ^{99m}Tc-MAA-Ad were highest whereby the liver-to-blood ratio peaked at

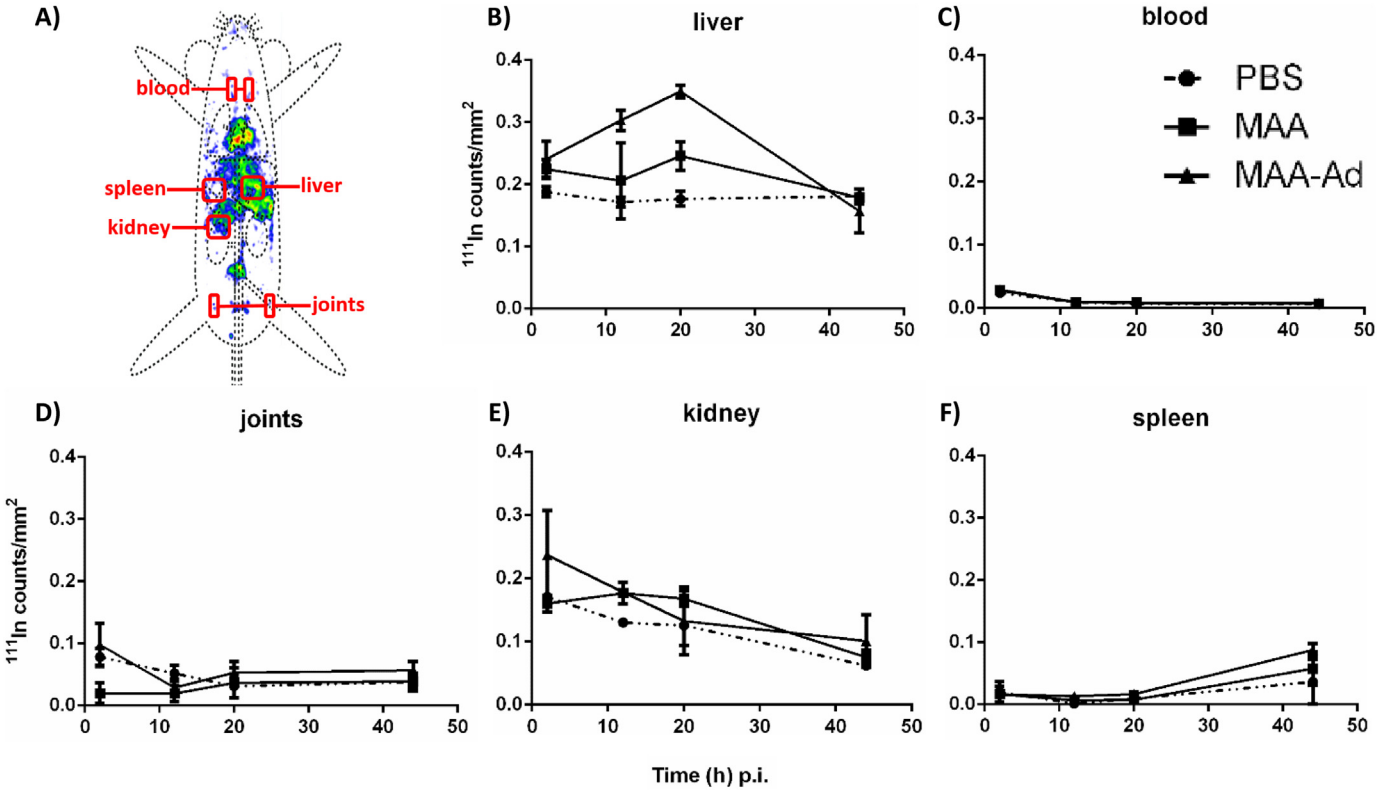

Fig. 4. Time-dependent uptake of ^{111}In-Cy5$_{0.5}$CD$_9$PIBMA$_{39}$ in various tissues based on A) radioactivity calculations in ROI's. Data are expressed as the ^{111}In radioactivity counts per mm^3 on the scintigrams in regions of interest (ROI's) drawn over B) liver, C) blood, D) joints, E) kidney, and F) spleen.

44 h p.i.

5.4. Fluorescence imaging

Ex vivo fluorescence imaging analysis of the biodistribution of the host vector in various excised tissues of mice pretargeted with guest vectors ^{99m}Tc-MAA-Ad and ^{99m}Tc-MAA revealed an intense fluorescence signal in the liver (Fig. 3C & Fig. 5D) at all time points after administration of the host (2.0–2.6 × 10^{10} p/s/cm^2/sr) which was highest for ^{99m}Tc-MAA-Ad compared to those for MAA (0.9–1.5 × 10^{10} p/s/cm^2/sr) or PBS (0.06–0.4 × 10^{10} p/s/cm^2/sr) which follows the trend as observed for radioactivity with ^{111}In-Cy5$_{0.5}$CD$_9$PIBMA$_{39}$. At 44 h p.i. all values dropped below 0.6 × 10^{10} p/s/cm^2/sr.

6. Discussion

In this study we demonstrated that supramolecular interactions can form stable host–guest complexes between the host vector ^{111}In-Cy5$_{0.5}$CD$_9$PIBMA$_{39}$ and guest vector ^{99m}Tc-MAA-Ad *in vitro* and *in vivo*. The stability of these complexes over longer time periods strengthens the case for supramolecular pre-targeting strategies for radioembolization. Corroborating our previous results [15], we did not observe lung shunting, an essential property to prevent side effects due to off-target delivery [2,11]. Since complex formation could be realized up until 20 h, the technology can accommodate single-session procedures whereby the host vector therapy is administered within hours after the scout scan (MAA-Ad; guest vector). In current clinical practice these procedures are performed several weeks apart [22]. A single-session procedure would be more patient-friendly as after the correct administration of the scout vector a therapeutic vector can be directly administered *via* the same catheter [23]. In addition to decreasing the invasiveness of the embolization procedure, cost reduction can also be achieved, as the secondary host vectors do not demand functionalization with relatively expensive (*e.g.*, ^{90}Y or ^{166}Ho) isotopes, but could also act as carrier for cheaper therapeutical isotopes such as rhenium-188 or lutetium-177 [24]. Uniquely for our approach is that isotope labelling could be converted into kit chemistry.

From SPECT images (Fig. 2A, B, Fig. 3A, B), biodistribution data (Fig. 4, 5, Table S1), and fluorescence imaging (Fig. 3C, Fig. 5D) it may be concluded that, while initially predominantly present in the blood, ^{111}In-Cy5$_{0.5}$CD$_9$PIBMA$_{39}$ actively co-localizes with the MAA-Ad guest vector in the liver, resulting in increased uptake up to 20 h p.i. In addition to this conclusion, the 12 h timepoint gave the most optimal liver-to-blood ratios; Figs. 2–4, Table S1). Clearly, the complex formation in the presence of MAA-Ad is unaffected by the strong serum interactions recorded for ^{111}In-Cy5$_{0.5}$CD$_9$PIBMA$_{39}$ (approximately 90%; Fig. S1).

It was found that unbound host vector was excreted *via* both renal and hepatic clearance; most likely the latter occurred *via* the reticuloendothelial system [25]. The hepatic clearance complicates accurate performance assessments of hepatic and spleen signals at the 44 h time point. Ideally, future versions of the host vector are synthetically refined so that uptake in radiation-sensitive background organs such as the kidneys is minimized. This development may be achieved by dose optimization for the host vector or fine-tuning the polymer's functional groups [26]; these optimizations can possibly help to control the pharmacokinetics including the serum binding properties. In drug efficacy studies, it is often considered critical to account for plasma protein binding as this relates to the availability of the free drug, its half-life, and its subsequent renal elimination [27]. The lack of pulmonary shunting suggests ^{99m}Tc-MAA-Ad particles remained confined in the liver and are not released into the vasculature (Fig. S1). Proteolytic breakdown of ^{99m}Tc-MAA-Ad as reported for pulmonary and hepatic injected ^{99m}Tc-MAA [28] was not observed in our experimental setup; no accumulation of unconjugated ^{99m}Tc-activity was observed in typical reservoir tissues, *e.g.*, thyroid, salivary glands and stomach [19]. This apparent increase in both MAA-Ad and MAA stability remains speculative, but we hypothesize that it could be attributed to a different

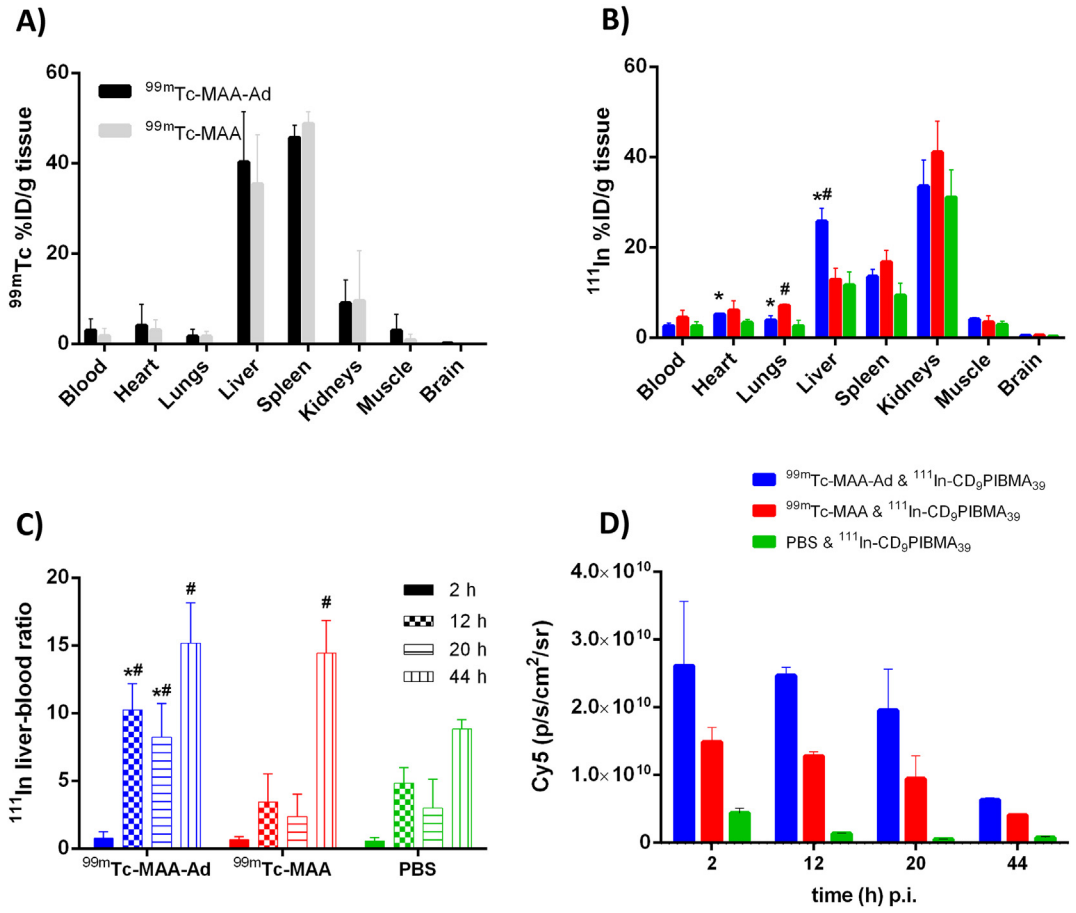

Fig. 5. A) The bio-distribution of guest vectors ^{99m}Tc-MAA-Ad and ^{99m}Tc-MAA at various intervals after local administration. Data (expressed as the mean ± SD of the percentage of the injected dose per gram tissue (%ID/g) of 3 observations were calculated based on the radioactive counts measured in indicated tissues at 12, and 20 h p.i. B) Biodistribution of intravenously administered ^{111}In-Cy5$_{0.5}$CD$_9$PIBMA$_{39}$ (host vector) 12 h after hepatic pre-targeting with guest vectors MAA-Ad (blue bars),MAA (red bars) or as control PBS (green bars). C) Dynamic hepatic uptake of IV administered host vector ^{111}In-Cy5$_{0.5}$CD$_9$PIBMA$_{39}$. Data are expressed as the mean ± SD ratios of the %ID/g in liver and blood measured at 2, 12, 20, and 44 h p.i. of the host vector. For all pre-targeting settings at 44 h p.i. liver-to-blood ratios for ^{111}In-Cy5$_{0.5}$CD$_9$PIBMA$_{39}$ are increased compared to the earlier intervals which is indicative for clearance of proteolytic or metabolic products. D) *Ex-vivo* fluorescence imaging analysis of the biodistribution of ^{111}In-Cy5$_{0.5}$CD$_9$PIBMA$_{39}$ in excised livers of mice pretargeted with ^{99m}Tc-MAA-Ad, ^{99m}Tc-MAA, or PBS at various intervals until 44 h p.i. The fluorescence signal is determined from regions of interest (ROI's) drawn over the liver. Data are expressed as the average radiance p/s/cm^2/sr after correction for background activity. * = $p < 0.01$ compared to ^{99m}Tc-MAA, # = p < 0.01 compared to PBS. (For interpretation of the references to colour in this figure legend, the reader is referred to the web version of this article.)

proteolytic breakdown pathway of aggregated human albumin particles in mice.

We observed long-term complex formation, which was affected by only two small factors of dissociation. Firstly, dissociation of $^{111}In^{3+}$ from the host vector occurred in the initial phase after intravenous injection, which was in line with the 5% dissociation observed *in vitro*. The use of dedicated chelators that support stable chelation of the radioisotope could prevent this effect [29]. Secondly, *in vitro* for [^{111}In-Cy5$_{0.5}$CD$_9$PIBMA$_{39}$-^{99m}Tc-MAA-Ad] a 20% complex dissociation was observed over a 44 h timespan, which was confirmed *in vivo* with the biodistribution assays. Indeed, a slow rate of excretion of about 20%/g for ^{111}In-Cy5$_{0.5}$CD$_9$PIBMA$_{39}$ was observed in this study. Again, future synthetic refinements could further address the stability by reducing the dissociation of the host vector and by improving the chelation of the radioisotope.

While serum–albumin binding is widely explored, clinical albumin-based nanodevices are more scarce [30]. Some examples are drug delivery of therapeutic agents with targeted albumin nanoparticles [31], ^{99m}Tc-labeled albumin colloids for the visualization of the lymphatic vessels [32], and surgical sentinel node detection with ICG-^{99m}Tc-nanocolloid [33]. With the presented radioembolization strategy we hope to promote the usage of biodegradable particles for nanomedicine [34]. Alternatively, the employed pre-targeting concept could be equally effective on different, *e.g.*, more spherical synthetic microparticles such as gold particles or quantum dots [35,36].

A debate with regard to radioembolization technologies on whether or not the agents should be classified as medical technology or drugs is ongoing. Despite being chemical in nature and the fact that these agents administer a radiation dose to a patient even when used incorrectly, commercial microspheres are considered a medical device. Although the practical steps during the application are similar and the components don't actively interact with the body's metabolic or immune system (the fact that it relies on supramolecular interactions) could mean the proposed technology would be considered as a drug by the designated authorities. In that case it would affect the cost of translation and the quality standards that have to be met. The composition of the microparticles used as pre-targeting platform could potentially influence this selection.

7. Conclusions

The reported dual-isotope multiplexing and fluorescence imaging data further underlines the potential of using multivalent host–guest interactions between Ad and CD on albumin-based nanodevices *in vivo*.

With that, a supramolecular tool has been created that could help address unmet clinical needs in the field of radioembolization.

Competing interests

The authors declare no competing of interest.

Data availability statement

The raw/processed data required to reproduce these findings cannot be shared at this time due to legal or ethical reasons and at this time as the data also forms part of an ongoing study.

Acknowledgements

We thank M.N. van Oosterom for his assistance with the reconstruction of the SPECT images, S.I. van Leeuwen for the schematic drawings and A.W. Hensbergen for critical reading of the manuscript. The research leading to these results was funded with grants from: the European Research Council (ERC) under the European Union's Seventh Framework Program FP7/2007-2013 (grant agreement number 2012-306890), from the Netherlands Organization for Scientific Research (VIDI-grant - STW BGT11272) and the 2015-2016 Postdoctoral Molecular Imaging Scholar Program Grant granted by the Society of Nuclear Medicine and Molecular Imaging (SNMMI, Eurostars project E! 11079 and the Education and Research Foundation (ERF) for Nuclear Medicine and Molecular Imaging.

Appendix A. Supplementary data

Supplementary data to this article can be found online at https://doi.org/10.1016/j.jconrel.2018.11.020.

References

[1] A. Forner, J.M. Llovet, J. Bruix, Hepatocellular carcinoma, Lancet 379 (9822) (2012) 1245–1255.
[2] F.E. Boas, L. Bodei, C.T. Sofocleous, Radioembolization of colorectal liver metastases: indications, technique, and outcomes, J. Nucl. Med. 58 (Supplement 2) (2017) 104S–111S.
[3] G.A. van Hazel, V. Heinemann, N.K. Sharma, M.P. Findlay, J. Ricke, M. Peeters, D. Perez, B.A. Robinson, A.H. Strickland, T. Ferguson, J. Rodriguez, H. Kroning, I. Wolf, V. Ganju, E. Walpole, E. Boucher, T. Tichler, E. Shacham-Shmueli, A. Powell, P. Eliadis, R. Isaacs, D. Price, F. Moeslein, J. Taieb, G. Bower, V. Gebski, M. Van Buskirk, D.N. Cade, K. Thurston, P. Gibbs, SIRFLOX: Randomized phase III trial comparing first-line mFOLFOX6 (plus or minus Bevacizumab) versus mFOLFOX6 (plus or minus Bevacizumab) plus selective internal radiation therapy in patients with metastatic colorectal cancer, J. Clin. Oncol. 34 (15) (2016) 1723–1731.
[4] H.S. Wasan, P. Gibbs, N.K. Sharma, J. Taieb, V. Heinemann, J. Ricke, M. Peeters, M. Findlay, A. Weaver, J. Mills, C. Wilson, R. Adams, A. Francis, J. Moschandreas, P.S. Virdee, P. Dutton, S. Love, V. Gebski, A. Gray, G. van Hazel, R.A. Sharma, First-line selective internal radiotherapy plus chemotherapy versus chemotherapy alone in patients with liver metastases from colorectal cancer (FOXFIRE, SIRFLOX, and FOXFIRE-Global): a combined analysis of three multicentre, randomised, phase 3 trials, Lancet Oncol. 18 (9) (2017) 1159–1171.
[5] D. Janevska, V. Chaloska-Ivanova, V. Janevski, Hepatocellular carcinoma: risk factors, diagnosis and treatment, Open Access. Maced. J. Med. Sci. 3 (4) (2015) 732–736.
[6] R. Duran, J. Chapiro, R.E. Schernthaner, J.F. Geschwind, Systematic review of catheter-based intra-arterial therapies in hepatocellular carcinoma: state of the art and future directions, Br. J. Radiol. 88 (1052) (2015) 20140564.
[7] B. Sangro, L. Carpanese, R. Cianni, R. Golfieri, D. Gasparini, S. Ezziddin, P.M. Paprottka, F. Fiore, M. Van Buskirk, J. Ignacio Bilbao, G. Maria Ettorre, R. Salvatori, E. Giampalma, O. Geatti, K. Wilhelm, R. Thorsten Hoffmann, F. Izzo, M. Iñarrairaegui, C. Ludovico Maini, C. Urigo, A. Cappelli, A. Vit, H. Ahmadzadehfar, T. Franz Jakobs, S. Lastoria, Survival after Yttrium-90 resin microsphere radioembolization of hepatocellular carcinoma across Barcelona clinic liver cancer stages: a European evaluation, Hepatology 54 (3) (2011) 868–878.
[8] R. Salem, R.J. Lewandowski, V.L. Gates, C.W. Nutting, R. Murthy, S.C. Rose, M.C. Soulen, J.-F.H. Geschwind, L. Kulik, Y.H. Kim, C. Spreafico, M. Maccauro, L. Bester, D.B. Brown, R.K.W. Ryu, D.Y. Sze, W.S. Rilling, K.T. Sato, B. Sangro, J.I. Bilbao, T.F. Jakobs, S. Ezziddin, S. Kulkarni, A. Kulkarni, D.M. Liu, D. Valenti, P. Hilgard, G. Antoch, S.P. Muller, H. Alsuhaibani, M.F. Mulcahy, M. Burrel, M.I. Real, S. Spies, A.A. Esmail, J.-L. Raoul, E. Garin, M.S. Johnson, A.B. Benson, R.A. Sharma, H. Wasan, B. Lambert, K. Memon, A.S. Kennedy, A. Riaz, Research reporting standards for radioembolization of hepatic malignancies, J. Vasc. Interv. Radiol. 22 (3) (2011) 265–278.
[9] R. Hickey, R.J. Lewandowski, T. Prudhomme, E. Ehrenwald, B. Baigorri, J. Critchfield, J. Kallini, A. Gabr, B. Gorodetski, J.-F. Geschwind, A. Abbott, R. Shridhar, S.B. White, W.S. Rilling, B. Boyer, S. Kauffman, S. Kwan, S.A. Padia, V.L. Gates, M. Mulcahy, S. Kircher, H. Nimeiri, A.B. Benson, R. Salem, 90Y radioembolization of colorectal hepatic metastases using glass microspheres: safety and survival outcomes from a 531-patient multicenter study, J. Nucl. Med. 57 (5) (2016) 665–671.
[10] L. Uliel, H.D. Royal, M.D. Darcy, D.A. Zuckerman, A. Sharma, N.E. Saad, From the angio suite to the γ-camera: Vascular mapping and 99mTc-MAA hepatic perfusion imaging before liver radioembolization - a comprehensive pictorial review, J. Nucl. Med. 53 (11) (2012) 1736–1747.
[11] A. Riaz, R. Awais, R. Salem, Side effects of Yttrium-90 radioembolization, Front. Oncol. 4 (198) (2014) 1–11.
[12] M. Xing, S. Lahti, N. Kokabi, D.M. Schuster, J.C. Camacho, H.S. Kim, 90Y Radioembolization lung shunt fraction in primary and metastatic liver cancer as a biomarker for survival, Clin. Nucl. Med. 41 (1) (2016) 21–27.
[13] E. Garin, Y. Rolland, S. Laffont, J. Edeline, Clinical impact of (99m)Tc-MAA SPECT/CT-based dosimetry in the radioembolization of liver malignancies with (90)Y-loaded microspheres, Eur. J. Nucl. Med. Mol. I. 43 (3) (2016) 559–575.
[14] M.T. Rood, S.J. Spa, M.M. Welling, J.B. Ten Hove, D.M. van Willigen, T. Buckle, A.H. Velders, F.W. van Leeuwen, Obtaining control of cell surface functionalizations via pre-targeting and supramolecular host guest interactions, Sci. Rep. 7 (2017) 39908.
[15] S.J. Spa, M.M. Welling, M.N. van Oosterom, D.D.D. Rietbergen, M.C. Burgmans, W. Verboom, J. Huskens, T. Buckle, F.W.B. van Leeuwen, A supramolecular approach for liver radioembolization, Theranostics 8 (9) (2018) 2377–2386.
[16] M. Palmowski, A. Goedicke, A. Vogg, G. Christ, G. Mühlenbruch, H.J. Kaiser, R.W. Günther, C.K. Kuhl, F.M. Mottaghy, F.F. Behrendt, Simultaneous dual-isotope SPECT/CT with ^{99m}Tc- and ^{111}In-labelled albumin microspheres in treatment planning for SIRT, Eur. Radiol. 23 (11) (2013) 3062–3070.
[17] H. Kasuya, D.K. Kuruppu, J.M. Donahue, E.W. Choi, H. Kawasaki, K.K. Tanabe, Mouse models of subcutaneous spleen reservoir for multiple portal venous injections to treat liver malignancies, Cancer Res. 65 (9) (2005) 3823–3827.
[18] M.M. Welling, A. Bunschoten, J. Kuil, R.G.H.H. Nelissen, F.J. Beekman, T. Buckle, F.W.B. van Leeuwen, Development of a hybrid tracer for SPECT and optical imaging of bacterial infections, Bioconjug. Chem. 26 (5) (2015) 839–849.
[19] Limits for Intakes of Radionuclides by Workers, Pergamon Press, Oxford, 1980.
[20] F.P. Castronovo Jr., H.N. Wagner Jr., Comparative toxicity and pharmacodynamics of ionic indium chloride and hydrated indium oxide, J. Nucl. Med. 14 (9) (1973) 677–682.
[21] E.H. Gilbert, J.D. Earle, E. Glatstein, M.L. Goris, H.S. Kaplan, J.P. Kriss, ^{111}indium bone marrow scintigraphy as an aid in selecting marrow biopsy sites for the evaluation of marrow elements in patients with lymphoma, Cancer 38 (4) (1976) 1560–1567.
[22] L. Sancho, M. Rodriguez-Fraile, J.I. Bilbao, C. Beorlegui Arteta, M. Iñarrairaegui, V. Moran, B. Sangro, Is a technetium-99m macroaggregated albumin scan esential in the workup for selective internal radiation therapy with yttrium-90? An analysis of 532 patients, J. Vasc. Interv. Radiol. 28 (11) (2017) 1536–1542.
[23] N. Rostambeigi, A.S. Dekarske, E.E. Austin, J. Golzarian, E.N. Cressman, Cost effectiveness of radioembolization compared with conventional transarterial chemoembolization for treatment of hepatocellular carcinoma, J. Vasc. Interv. Radiol. 25 (7) (2014) 1075–1084.
[24] M. Lyra, A. Georgantzoglou, S. Kordolaimi, N. Lagopati, A. Ploussi, A. Salvara, I. Vamvakas, Radioisotopes Production and Dosimetry, Nuclear Medicine Therapy, Hellenic Association of Medical Physicists, Athens, Greece, 2011.
[25] R. Lang, X. Jun-Hua, C. Bo, L. Huiqin, L. Ming, J. Yan, X. Liang, G. Shi-Shang, L. Wei, Z. Xing-Zhong, Synthetic nanoparticles camouflaged with biomimetic erythrocyte membranes for reduced reticuloendothelial system uptake, Nanotechnology 27 (8) (2016) 085106.
[26] F. Alexis, E. Pridgen, L.K. Molnar, O.C. Farokhzad, Factors affecting the clearance and biodistribution of polymeric nanoparticles, Mol. Pharm. 5 (4) (2008) 505–515.
[27] D.A.J. Bow, J.L. Perry, J.D. Simon, J.B. Pritchard, The impact of plasma protein binding on the renal transport of organic anions, J. Pharmacol. Exp. Ther. 316 (1) (2006) 349–355.
[28] O.S. Grosser, J. Ruf, D. Kupitz, A. Pethe, G. Ulrich, P. Genseke, K. Mohnike, M. Pech, W.S. Richter, J. Ricke, H. Amthauer, Pharmacokinetics of 99mTc-MAA- and 99mTc-HSA-microspheres used in Preradioembolization Dosimetry: Influence on the Liver-Lung Shunt, J. Nucl. Med. 57 (6) (2016) 925–927.
[29] R. Schibli, A.P. Schubiger, Current use and future potential of organometallic radiopharmaceuticals, Eur. J. Nucl. Med. Mol. Imaging 29 (11) (2002) 1529–1542.
[30] A. Loureiro, N. G. Azoia, A. C. Gomes, A. Cavaco-Paulo, Albumin-based nanodevices as drug carriers, Curr. Pharm. Des. 22 (10) (2016) 1371–1390.
[31] H. Kouchakzadeh, M.S. Safavi, S.A. Shojaosadati, Efficient delivery of therapeutic agents by using targeted albumin nanoparticles, Adv. Protein Chem. Struct. Biol. 98 (2015) 121–143.
[32] N.S. Van den Berg, T. Buckle, G.I. Kleinjan, W.M. Klop, S. Horenblas, H.G. Van der Poel, R.A. Valdes-Olmos, F.I. Van Leeuwen, Hybrid tracers for sentinel node biopsy, Q. J. Nucl. Med. Mol. Imag. 58 (2) (2014) 193–206.
[33] G.H. KleinJan, E. van Werkhoven, N.S. van den Berg, M.B. Karakullukcu, H. Zijlmans, J.A. van der Hage, B.A. van de Wiel, T. Buckle, W.M.C. Klop, S. Horenblas, R.A. Valdes Olmos, H.G. van der Poel, F.W.B. van Leeuwen, The best of both worlds: a hybrid approach for optimal pre- and intraoperative identification of sentinel lymph nodes, Eur. J. Nucl. Med. Mol. Imaging 45 (11) (2018)

1915–1925.
[34] M. Jamre, M. Shamsaei, M. Erfani, S. Sadjadi, M. Ghannadi Maragheh, Preparation and evaluation of ^{188}Re sulfide colloidal nanoparticles loaded biodegradable poly (L-lactic acid) microspheres for radioembolization therapy, J. Label. Compd. Radiopharm. 61 (8) (2018) 586–594.
[35] M.-C. Daniel, D. Astruc, Gold nanoparticles: assembly, supramolecular chemistry, quantum-size-related properties, and applications toward biology, catalysis, and nanotechnology, Chem. Rev. 104 (1) (2004) 293–346.
[36] Y. Liu, H. Wang, Y. Chen, C.-F. Ke, M. Liu, Supramolecular aggregates constructed from gold nanoparticles and l-Try-CD polypseudorotaxanes as captors for fullerenes, J. Am. Chem. Soc. 127 (2) (2005) 657–666.